IEEE Photonics Journal
An IEEE Photonics Society Publication

Open Access

Refractive Index Nanosensor With Simple Structure Based on Fano Resonance

Volume 12, Number 4, August 2020

Jing Guo
Xiaoyu Yang
Yifei Wang
Mengmeng Wang
Ertian Hua
Shubin Yan

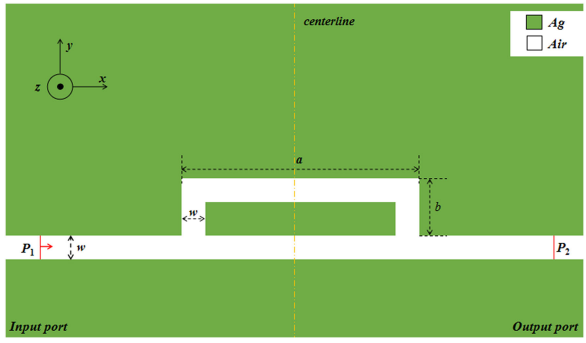

DOI: 10.1109/JPHOT.2020.3015988

Refractive Index Nanosensor With Simple Structure Based on Fano Resonance

Jing Guo,[1] Xiaoyu Yang ,[1,2] Yifei Wang,[2] Mengmeng Wang,[2] Ertian Hua,[1] and Shubin Yan [1]

[1]School of Electrical Engineering, Zhejiang University of Water Resources and Electric Power, Key Laboratory for Technology in Rural Water Management of Zhejiang Province, Hangzhou 310018, China
[2]School of Instrument and Electronics, North University of China, Taiyuan 030051, China

DOI:10.1109/JPHOT.2020.3015988

Manuscript received May 28, 2020; revised August 4, 2020; accepted August 7, 2020. Date of publication August 12, 2020; date of current version August 25, 2020. This work was supported in part by the National Natural Science Foundation of China under Grants 61675185, 61875250, 61975189, in part by the Natural Science Foundation of Shanxi Province under Grants 201601D011008, and in part by the Fund for Shanxi '1331 Project' Key Subject Construction. *(Jing Guo and Xiaoyu Yang contributed equally to this work.)* Corresponding author: Shubin Yan (e-mail: yanshb@zjweu.edu.cn)

Abstract: Herein, a refractive-index sensor is theoretically proposed, which comprises metal-insulator-metal waveguide and single rectangle cavity without a long side (RCWALS). The propagation characteristics were analyzed by finite element method. Compared with the contrastive structure, the designed single RCWALS structure has better transmission spectra and stronger resonance and supports Fano resonance. The effects of the structural parameters on sensing characteristics were investigated. Mode 1 of single RCWALS structure has better performance parameter, which is the best sensitivity of 1840 nm/RIU with a figure of merit of 51.11. Additionally, three derived structures are presented, which are composed of MIM waveguide and two RCWALS in different positions. They have lower sensitivity but better figure of merit, and provide more detection positions. The designed structures, which are greatly simple, can potentially apply to nanophotonics.

Index Terms: Metal-insulator-metal, Fano resonance, refractive-index nanosensor, finite element method.

1. Introduction

Surface plasmon polaritons (SPPs) are charge-density waves, which are largely trapped on metal-dielectric interface and can transmit along the interface [1], [2]. In addition, SPPs can get over the classical diffraction of light limit and control light within nanoscale [3], [4]. Thus, various photonic devices based on SPPs were extensively reported, for instance, filters [5]–[7], optical switching [8], [9], splitters [10], [11], nanosensors [12]–[15], and demultiplexers [16]. Among this, SPPs-based nanosensor is an important application, which has advantages of smaller size as well as being easy to integrate into optical circuits and get in touch with sensing mediums. However, comparing with fiber sensors, SPPs-based sensors have lower sensitivity [17]. Therefore, one significant factor for designing an SPPs-based sensor is improving its sensitivity. In addition, numerous interesting optical phenomena were observed in plasmon coupled structures, for example, plasmon-induced transparency (PIT) [18] and Fano resonance [19]–[21]. Fano resonance has wide application because it emerges an asymmetric sharp outline and displays comparatively narrow full width at half maximum (FWHM) [22]. As a result, Fano resonance has great optical resolution, which

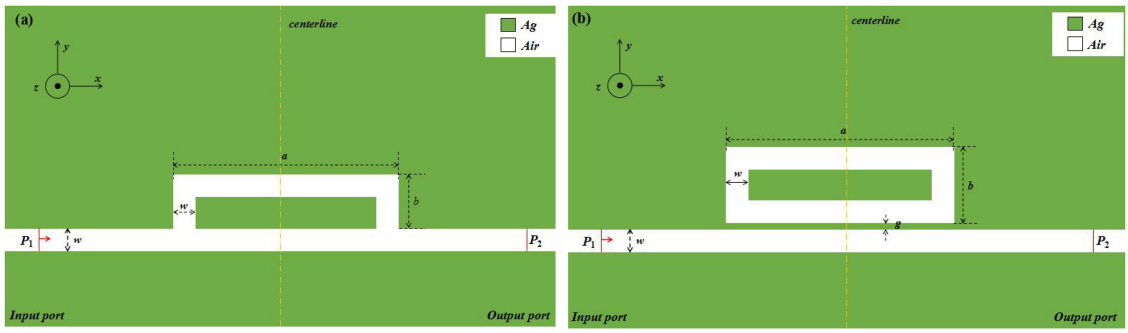

Fig. 1. 2D schematics of (a) designed single RCWALS structure and (b) contrastive structure.

means that its peak or dip wavelength is easy to tell from the wavelength of other positions. Also, different geometry structures or mediums environments could largely lead to the change of dip or peak position of Fano resonance.

The metal-insulator-metal (MIM) waveguides, a kind of SPPs-based waveguides, have extraordinary properties, for example, shorter transmission length, easy fabrication, stronger localized field confinement, smaller dimension, and low propagation loss [23], [24]. Thus, the combination of Fano resonance and MIM coupled system could accomplish great sensitivity with a small size. So far, plenty of sensors based on the combination have been widely investigated. Yan *et al.* [25] designed a nanosensor with sensitivity of 1071.4 nm/RIU, which comprises one stub and one notched ring resonator. Yun *et al.* [26] presented a refractive-index sensor consisting of stub coupled with square resonator, which could obtain the sensitivity of 938 nm/RIU. Zhang *et al.* [27] proposed coupled structure of double rectangle cavities and MIM waveguide, whose sensitivity is 596 nm/RIU. This proposed nanosensor with simpler structure can achieve a high sensitivity of 1840 nm/RIU.

In this paper, the simple-structure refractive-index nanosensor comprises a MIM waveguide and single rectangle cavity without a long side (RCWALS). Lots of works studied circular ring cavity [15], [17], [25], however, less work investigated the rectangular ring cavity, which is discussed in this paper. Besides, the horizontal size and vertical size of circular ring cavity have to change at the same time, which may not suit some size-required devices. Nevertheless, in rectangular ring cavity, we can only change horizontal size or vertical size, which can satisfy the requirement of some special size devices. The propagation characteristics were demonstrated by the finite element method (FEM). A contrastive structure was employed for proving superiority of designed single RCWALS structure. Moreover, it is known that diverse geometric parameters would lead to different transmission spectra, sensitivity, and FWHM. Therefore, the influence of structural parameters was studied in detail, which include the long side of RCWALS and the short side of RCWALS. Additionally, three derived structures are presented, and their sensing characteristics were investigated.

2. Geometry Model and Analysis Method

The designed single RCWALS structure and contrastive structure are plotted in Fig. 1(a) and 1(b), respectively. The single RCWALS structure is composed of a MIM waveguide and single rectangle cavity without a long side (RCWALS). The contrastive structure is used to analyze the superiority of the designed single RCWALS structure, which comprises a MIM waveguide and single rectangle cavity. These two structures have the same geometric parameters, and they are both symmetrical about the centerline. The long side of rectangle cavity and RCWALS is described by a. The short side of rectangle cavity and RCWALS is defined as b. And the width of the rectangle, RCWALS and MIM waveguide remains unaltered (i.e. $w = 50$ nm), which is greatly shorter than wavelength of input light. Thus, the coupled system only excites fundamental transverse magnetic (TM_0) mode

[28], which could generate SPP waves. The coupling distance between waveguide and rectangle cavity is expressed by *g*. The silver is selected as the filled metal, which is due to its fewer power-consumed. The silver and air are denoted by green and white districts in Fig. 1, respectively. The relative permittivity of air is $\varepsilon_d = 1$, the relative permittivity of silver is attained by the Debye–Drude dispersion model [29]:

$$\varepsilon(\omega) = \varepsilon_\infty + \frac{\varepsilon_s - \varepsilon_\infty}{1 + i\tau\omega} + \frac{\sigma}{i\omega\varepsilon_0} \tag{1}$$

Where the relative permittivity of infinite frequency is taken as $\varepsilon_\infty = 3.8344$, the static permittivity is expressed by $\varepsilon_s = -9530.5$, the conductivity of silver is denoted as $\sigma = 1.1486 \times 10^7$ S/m, and the relaxation time is defined as $\tau = 7.35 \times 10^{-15}$ s.

The z-direction dimension of silver film of presented structure is 100 nm, which is hugely smaller than light wavelength. Therefore, 3D model can be simplified to 2D model without too much departure, which can satisfy the limitation of computer workstation and be easy to illustrate the structure. The COMSOL Multiphysics 5.3a is employed to construct the geometric model. The perfect matched layer serves as absorbing boundary condition in all boundaries. And ultra-fine meshing is opted to guarantee the simulation precision. This structure can be manufactured by focused ion beam (FIB) method. To be specific, the focused ion beam is sputtered on the silver film to form the nanostructure. However, there are some challenges of FIB method, such as lower production and limited selection of materials. Besides, the focused ion beam has to sputter in the right position. Otherwise, the fabricated nanostructure will have some departures that maybe affect the sensitivity of sensor. P_1 and P_2 respectively represent input port and output port. The light from light source (e.g. laser) can be coupled into P_1 by nanofiber, and the light at P_2 can go through the nanofiber and then be detected by Confocal Raman Microscopy [17]. The transmittance (T) is defined as $T = P_{out}/P_{in}$, where the input power P_{in} and output power P_{out} are expressed by integral values of energy flux density. Additionally, the SPPs can only couple into RCWALS when the resonance condition is satisfied [30], which is calculated by $\Delta\varphi = 2\pi m$. Where m is mode number, which is a positive integer (i.e. m = 1, 2, …). The resonance wavelength (λ_r) is expressed by [31], [32]:

$$\lambda_r = \frac{2L\mathrm{Re}(n_{eff})}{m - \phi_{ref}/\pi} \tag{2}$$

Where *L* is effective length of resonator, Re(n_{eff}) is the real part of effective refractive index, φ_{ref} is the phase shift of SPP reflection at the cavity metal wall.

3. Simulations and Results

To reveal the superiority of designed single RCWALS structure, the propagation properties were studied. The structural parameters of these two structures were set as follows: $g = 10$ nm, $a = 540$ nm, $b = 90$ nm. As shown in Fig. 2, transmission spectra for single RCWALS structure and contrastive structure are expressed by the pink and purple curves, respectively. As for the single RCWALS structure, it had three dips in the transmission spectrum. All the three dips had extremely low transmittance, and two dips (mode 1 and mode 2) had narrower FWHM. The extremely low transmittance results in great transmission contrast ratio. Comparatively narrow FWHM is the reason for small optical resolution and better figure of merit (FOM). As for the contrastive structure, it had four dips in the transmission spectrum. Only one dip (mode 1') had extremely low transmittance, and all dips had relatively broad FWHM, which indicates that the lineshape of contrastive structure is Lorentzian profile. However, the two narrower dips of the single RCWALS structure displayed a sharp asymmetrical shape, which implies that a phenomenon of Fano resonance occurred in the single RCWALS structure.

To better illustrate inner mechanism of the structures, the normalized H_Z field distributions of single RCWALS structure and contrastive structure at resonance dips were calculated. The

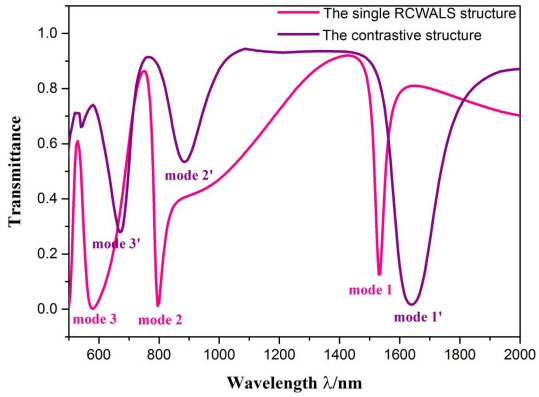

Fig. 2. Transmission spectra of the designed single RCWALS structure (pink line) and the contrastive structure (purple line).

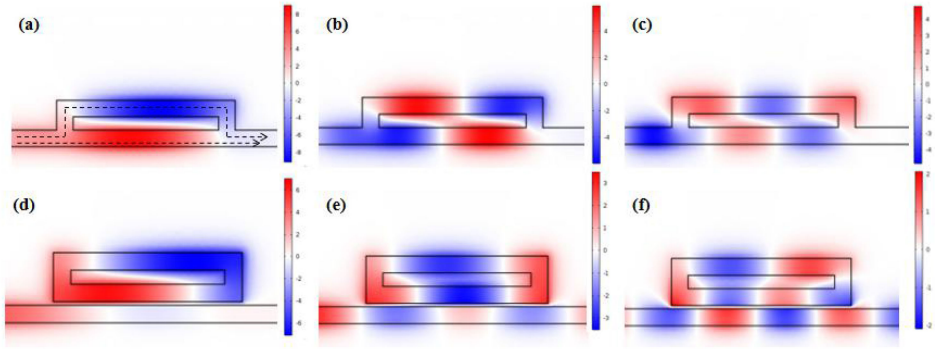

Fig. 3. The H_Z field distribution of (a) single RCWALS structure at $\lambda = 1530$ nm (mode 1). (b) single RCWALS structure at $\lambda = 795$ nm (mode 2). (c) single RCWALS structure at $\lambda = 580$ nm (mode 3). (d) contrastive structure at $\lambda = 1640$ nm (mode 1'). (e) contrastive structure at $\lambda = 885$ nm (mode 2'). (f) contrastive structure at $\lambda = 670$ nm (mode 3').

normalized H_Z field distributions of mode 1 ($\lambda = 1530$ nm), mode 2 ($\lambda = 795$ nm), mode 3 ($\lambda = 580$ nm) of single RCWALS structure are plotted in Fig. 3(a), 3(b), 3(c), respectively. It is observed that mode 1 had two nodes, mode 2 had four nodes, and mode 3 had six nodes. Also, the strength of normalized H_Z field of RCWALS of mode 1 was stronger than that of mode 2, and that of mode 2 was stronger than that of mode 3. These phenomena result from the diverse coupling strength between the bus waveguide and RCWALS in different resonance wavelength. The normalized H_Z field distributions of mode 1' ($\lambda = 1640$ nm), mode 2' ($\lambda = 885$ nm), mode 3' ($\lambda = 670$ nm) of contrastive structure are depicted in Fig. 3(d), 3(e), 3(f), respectively. Noticeably, mode 1' had two nodes, mode 2' had four nodes, and mode 3' had six nodes. Furthermore, similarly, the strength of normalized H_Z field of rectangle cavity of mode 1' was stronger than that of mode 2', and that of mode 2' was stronger than that of mode 3'. This indicates that mode 1, 2, 3 of single RCWALS structure are corresponding to mode 1', 2', 3' of contrastive structure. However, the nodes positions of mode 1 and 1', mode 2 and 2', mode 3 and 3' were different, respectively. This indicates that the inner mechanism was changed when contrastive structure changed to the designed structure, which induces that the strength of normalized H_Z field of mode 1, 2, 3 was stronger than that of mode 1', 2', 3', respectively (see Fig. 3). This demonstrates that more light was coupled into RCWALS to form a stronger standing wave when the single RCWALS structure was employed. Therefore, a stronger resonance was aroused in the RCWALS comparing with the contrastive structure, which could facilitate the occurrence of Fano resonance. Moreover, as shown

in Fig. 3(a) or 3(b), the SPPs could be supported at the interface of P_1, and then it would propagate into the bus waveguide. Most of them would be coupled into RCWALS when wavelength reaches resonance wavelength. It can form standing wave to confine the SPPs in the RCWALS to achieve ultra-low transmittance. It is also worth noting that SPPs are coupled into waveguide directly, which could be seen as continuum bright state. Because the transmission spectrum of waveguide is a horizontal line with same transmittance, which has wide bandwidth. In addition, SPPs are coupled into RCWALS indirectly, which could be seen as discrete dark state. Because the SPPs can only be coupled into the RCWALS when resonance condition is satisfied, which leads to a discrete transmission spectrum of RCWALS. Thus, when wavelength reaches resonance wavelength, there are two light pathways in the structure. As schematically shown in Fig. 3(a), one is from P_1 to P_2 by waveguide, which is in continuum bright state. The other is from P_1 to P_2 by RCWALS, which is in discrete dark state. These two light pathways interfere with each other, which induces the Fano resonance.

From the above analysis, it can be concluded that the single RCWALS structure, compared with the contrastive structure, has various advantages, such as relatively narrow FWHM and extremely low transmittance at some dips of transmission spectrum, stronger resonance in the RCWALS, and formation of Fano resonance. However, the mode 3 of the single RCWALS structure has relatively board FWHM, which induces a larger optical resolution and lower FOM. Thus, it would not continue to study in the following work. In other words, mode 1 and mode 2 of the single RCWALS structure, which have better properties, are investigated in the following of this paper.

There are two considerable parameters to judge performance of sensor, which are sensitivity (S) and figure of merit (FOM). One is calculated by $S = \Delta\lambda/\Delta n$, in which $\Delta\lambda$ is variation of dip wavelength and Δn is change of refractive indices. The other is calculated by FOM = S/FWHM [33]. Especially, FOM has two ways to express, and values of FOM obtained by above way are significantly smaller than that by the other way. In addition, one of Fano resonance advantages is that the position of Fano resonance is highly sensitive to diverse refractive indices, which is due to the sharp shape of Fano resonance. Thus, the effects of different refractive index on propagation characteristics were investigated. The geometric parameters were set as the same as Fig. 2. The refractive indices were adjusted from 1.00 to 1.05 RIU in the steps of 0.01 RIU. Noticeably, the refractive index is an abstract physical quantity, which can not be changed directly. However, many concrete physical quantities have relationship with refractive index so that refractive index can be changed by varying these physical quantities. On the other hand, some physical quantities, such as temperature, air pressure and concentration of hemoglobin level, can be indirectly detected by detecting refractive index. It indicates that this nanostructure can act as nanosensor to detect other physical quantities that are related to refractive index. Especially, as blood sample fills into RCWALS, this device is viable for biological sensing to detect the concentration of hemoglobin level. And the blood can be removed by blood-clean machine, so this device is reusable. However, as mentioned before, the designed structure is nanoscale so that the current cost of fabrication is relatively high. But nanomanufacturing technology is developing rapidly, so the cost will decrease in the near future. It is seen from Fig. 4(a) that the transmission spectra displayed an evident redshift with the increase of refractive index, which is consistent with Formula 2. To be specific, as refractive index increases, the $\mathrm{Re}(n_{\mathrm{eff}})$ rises. Then it leads to the increase of resonance wavelength, indicating that resonance wavelength shifts to the longer direction (i.e. redshift). Besides, the shape of transmission spectra almost maintained unaltered with the change of refractive indices.

The sensitivity of mode 1 is plotted in Fig. 4(b). Evidently, the shift of wavelength varied linearly as the variation of refractive indices altered. Additionally, the sensitivity can be attained, which is 1540 nm/RIU. The sensitivity of mode 2 is shown in Fig. 4(c). It is observed that the shift of wavelength also varied linearly as the change of refractive indices altered. Besides, the sensitivity of mode 2 is 760 nm/RIU, which is much smaller than the sensitivity of mode 1. Therefore, it is striking that mode 1 is more suitable as the detection position. Thus, mode 1 is continued to discuss in the following.

Although the proposed structure is simple, its structural parameters may affect the propagation properties, sensitivity and FWHM. Therefore, the geometric parameters of the sensor were

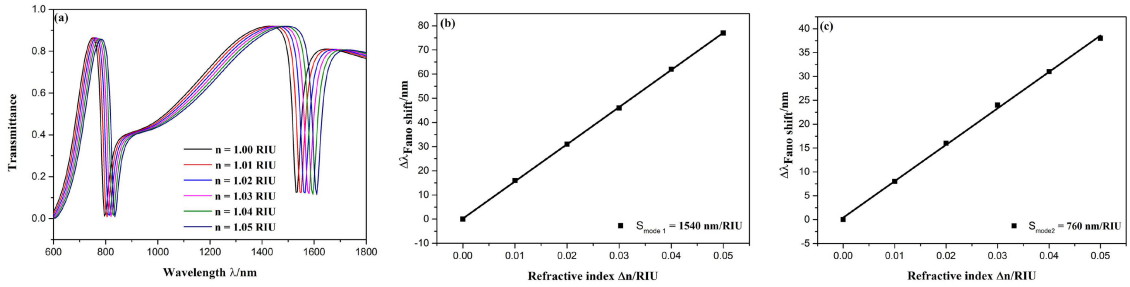

Fig. 4. The influence of different refractive index on transmission properties. (a) Transmission spectra for diverse refractive-index. (b) fitting line of mode 1 sensitivity. (c) fitting line of mode 2 sensitivity.

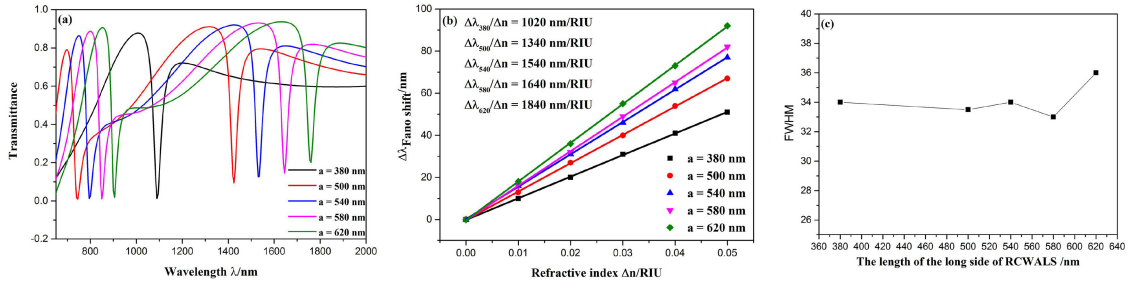

Fig. 5. The influence of different long side of RCWALS on transmission properties. (a) Transmission spectra for diverse long side of RCWALS. (b) the varying sensitivity of mode 1 with variation of long side of the RCWALS. (c) the FWHM change of mode 1 with increase of long side of the RCWALS.

investigated. First of all, the effects of long side of the RCWALS were discussed. The long side of RCWALS a was gradually set as 380, 500, 540, 580, 620 nm while keeping $b = 90$ nm. The transmission spectra can be seen from Fig. 5(a). As a became larger, the transmittance of dip slightly increased, the dip position exhibited a distinct redshift. This can be explained by Formula 2. The long side of RCWALS is effective length of the resonator. Therefore, the increase of a (i.e. the increase of L) induces the growth of resonance wavelength (i.e. redshift of resonance wavelength). Besides, no matter how a changed, the shape of transmission spectra almost remained steady. Additionally, as shown in Fig. 5(b), when a increased, the sensitivity of mode 1 got more excellent. Furthermore, the FWHM change of mode 1 with increase of the long side of RCWALS is depicted in Fig. 5(c). It is found that the FWHM varied slightly, which is in the range from 33 to 36. And when $a = 580$ nm, the FWHM obtained the minimum value. Overall, the longer a led to position movement and higher transmittance of dip and better sensitivity, but it had little influence on the shape of transmission spectra and FWHM. Therefore, it is indispensable to choose better structural parameters to balance transmittance, devise horizontal dimension and sensitivity. To be specific, larger long side of RCWALS induces higher sensitivity and higher transmittance. The change degree of sensitivity is bigger than that of transmittance. And the effect of sensitivity on sensor performance is more significant than that of transmittance. Hence, the larger long side of RCWALS should be selected to improve the sensitivity if the horizontal dimension is in the allowable range. By comprehensively considering the above factors, the best performance of this sensor is attained, which is 1840 nm/RIU with an FOM of 51.11.

Successively, the influence of short side of RCWALS was investigated. The short side of RCWALS b was gradually set as 70, 80, 90, 100, 110 nm, and the long side of RCWALS a was constantly equal to 540 nm. The transmission spectra are depicted in Fig. 6(a). As the short side of RCWALS became longer, the dip position almost remained unchanged except when $b = 70$ nm. Besides, as the short side of RCWALS increased, the shape of transmission spectra changed

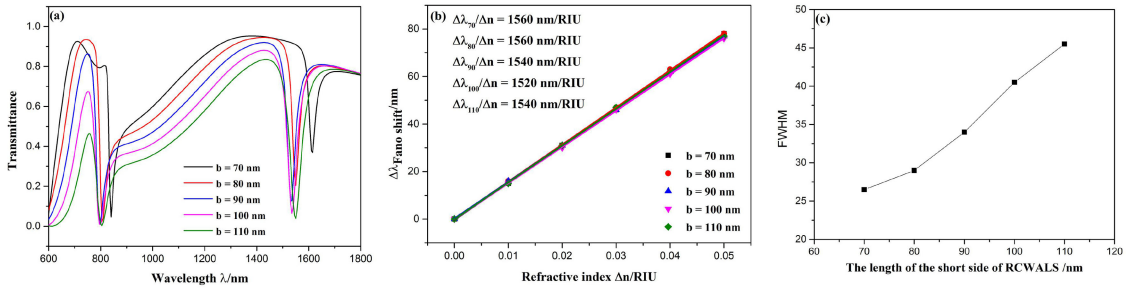

Fig. 6. The influence of different short side of RCWALS on transmission properties. (a) Transmission spectra for diverse short side of RCWALS. (b) the varying sensitivity of mode 1 with variation of short side of the RCWALS. (c) the FWHM change of mode 1 with increase of short side of the RCWALS.

from asymmetric narrow shape to almost symmetric broad shape, the transmittance of mode 1 reduced. Note that the transmission spectrum of $b = 70$ nm was much different from that of others. This is because the distance between waveguide and long side of RCWALS was so short that a interference between them happened when $b = 70$ nm. Moreover, as shown in Fig. 6(b), the short side of RCWALS b had less influence on sensitivity, which is in the range from 1520 nm/RIU to 1560 nm/RIU. In addition, as plotted in Fig. 6(c), the FWHM of mode 1 got larger with increase of the short side of RCWALS. It is known that smaller FWHM leads to better optical resolution, and excellent FOM depends on higher sensitivity and narrower FWHM. Hence, it is essential to make a tradeoff among devise longitudinal dimension, transmittance, and FWHM. Especially, when short side of RCWALS increased, the transmittance dropped slightly except $b = 70$ nm, the FWHM grew dramatically. And the importance of FWHM to affect the properties of sensor is bigger than that of transmittance. Thus, smaller short side of RCWALS should be chosen as long as it is not smaller than 70 nm to reduce the interference between waveguide and long side of RCWALS.

4. Derived Structures and Their Propagation Properties

Three derived structures are presented, which are depicted in Fig. 7(a), 7(c), 7(e), respectively. The derived structure 1 is symmetric about the centerline, which comprises a MIM waveguide coupled with two symmetric RCWALS. The derived structure 2 is composed of a MIM waveguide and two asymmetric RCWALS. The centerline of upper RCWALS and nether RCWALS's left short side is the same, while the centerline of nether RCWALS and upper RCWALS's right short side is the same. The derived structure 3 is centrosymmetric, which consists of a MIM waveguide and two centrosymmetric RCWALS. The geometry parameters of these three derived structures are the same as Fig. 2. Their transmission spectra and H_Z field distribution at dips were investigated, which are plotted in Fig. 7(b), 7(d), 7(f), respectively. Obviously, the three derived structures all had two modes. To illustrate the modes clearly, m (x, y) is defined to express the modes, where x means the order of mode and y denotes the number of derived structures. As for derived structure 1, Fano resonance emerged at m (1,1) ($\lambda = 1470$ nm) and m (2,1) ($\lambda = 760$ nm), which both had relatively narrow FWHM. Although m (2,1) had lower transmittance, m (1,1) had better transmission contrast ratio. There were three nodes at m (1,1), whereas there were six nodes at m (2,1). As for derived structure 2, Fano resonance was only supported at m (1,2) ($\lambda = 1350$ nm), which had narrower FWHM and larger transmission contrast ratio. The shape of m (2,2) ($\lambda = 785$ nm) was not sharp, hence it does not suit to be the detection point. The m (1,2) had four nodes, while m (2,2) had seven nodes. As for derived structure 3, m (1,3) ($\lambda = 1555$ nm) and m (2,3) ($\lambda = 825$ nm) had ultra-low transmittance, but none of its modes excited Fano resonance. There were four nodes at m (1,3), whereas there were eight nodes at m (2,3). Besides, compare nodes position of upper RCWALS of derived structures with that of single RCWALS structure, the nodes position of m (1,1), m (1,3) and mode 1 are the same, whereas the nodes position of m (1,2) and mode 1 are

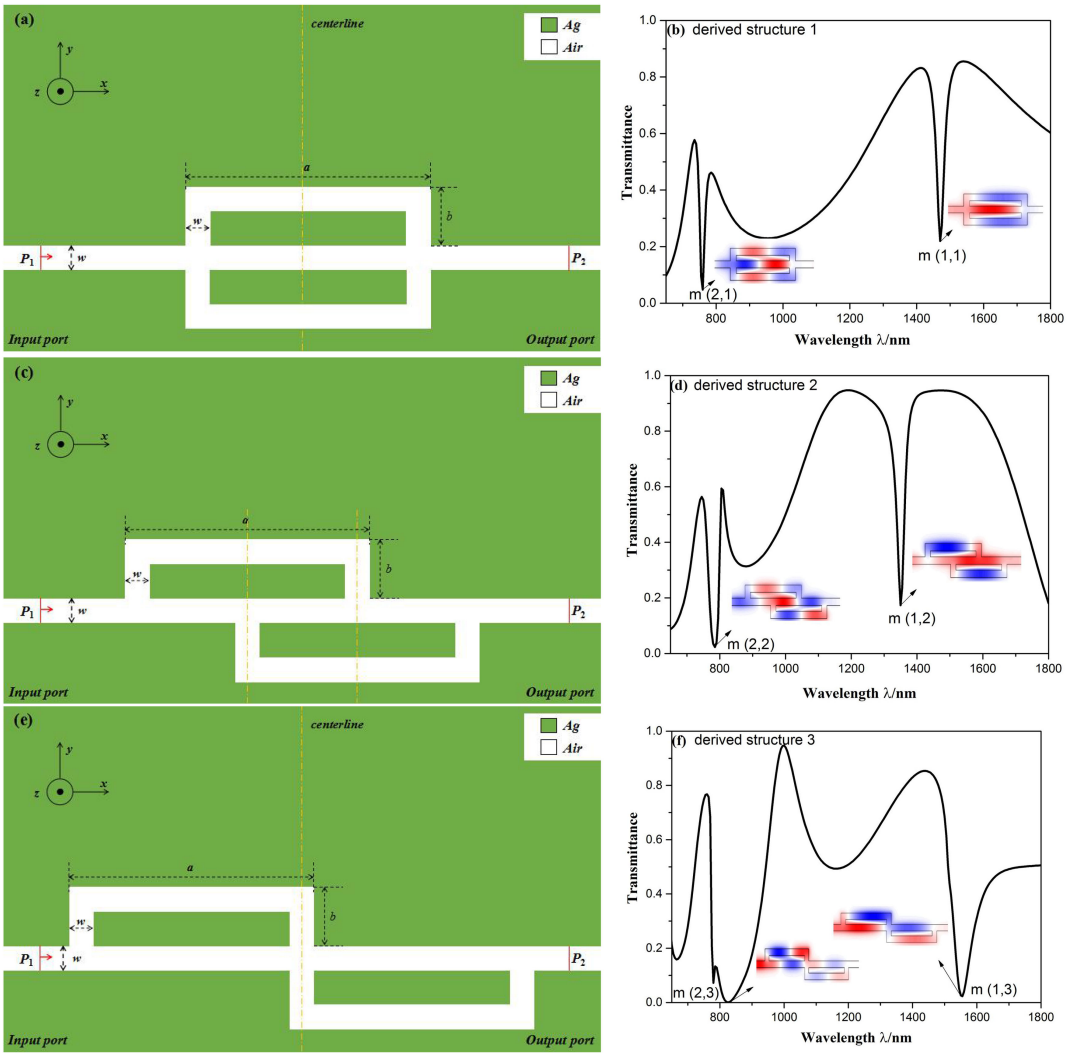

Fig. 7. The schematics and transmission properties of derived structures. (a) 2D schematics of derived structure 1. (b) Transmission spectrum of derived structure 1; The H_Z field distributions of m (1,1) and m (2,1) are depicted in the inset. (c) 2D schematics of derived structure 2. (d) Transmission spectrum of derived structure 2; The H_Z field distributions of m (1,2) and m (2,2) are depicted in the inset. (e) 2D schematics of derived structure 3. (f) Transmission spectrum of derived structure 3; The H_Z field distributions of m (1,3) and m (2,3) are depicted in the inset.

different. And the nodes positions of m (2,1), m (2,2), m (2,3) and mode 2 are all the same. It indicates that symmetric and centrosymmetric structures have similar H_Z filed distribution. We kept the position of upper RCWALS steady, it is evident that the nether RCWALS of derived structure 2 moved to the right compared with that of derived structure 1. And derived structure 3 is extreme movement situation of nether RCWALS. In conclusion, as the nether RCWALS moved to the right, the transmittance decreased but FWHM of spectra became broad. Additionally, the dip position was at diverse wavelength with right movement of nether RCWALS, which can apply for detection in different situations. According to above analysis, m (1,1) and m (1,2) have better performance. Thus, their detailed characteristics are discussed in the following.

The transmission spectra for diverse refractive indices (from 1.00 to 1.05 RIU) of m (1,1) and m (1,2) are shown in Fig. 8(a) and 8(b), respectively. It can be observed that they had similar changes with growing of refractive indices. Specifically speaking, when refractive indices rose, they

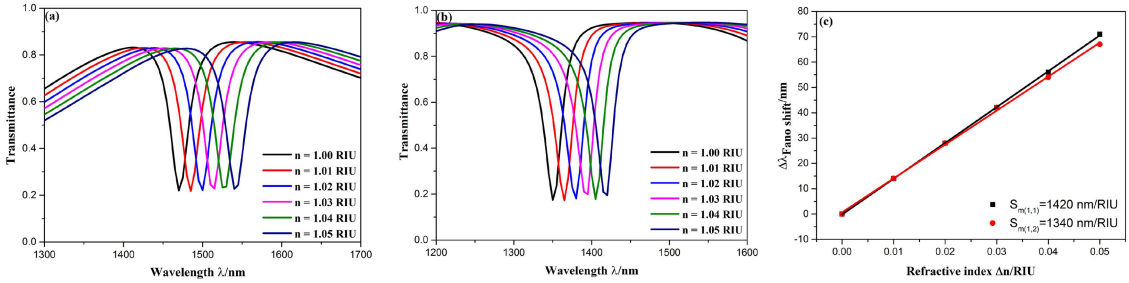

Fig. 8. The influence of different refractive index on transmission properties of m (1,1) and m (1,2). (a) Transmission spectra for diverse refractive indices of m (1,1). (b) Transmission spectra for diverse refractive indices of m (1,2). (c) the fitting line of sensitivity of m (1,1) and m (1,2).

both showed an apparent redshift, their shape of transmission spectra and transmittance at dips kept altered. It indicates that m (1,1) and m (1,2) can apply as detection points. Their sensitivities were also studied, which are plotted in Fig. 8(c). It is found that the sensitivities of m (1,1) and m (1,2) are respectively 1420 nm/RIU and 1340 nm/RIU, which are both lower than the sensitivity (1540 nm/RIU) of the single RCWALS structure in same geometric parameters. However, the FOM of m (1,1) is 56.13 and the FOM of m (1,2) is 47.85, which are both higher than the FOM (45.29) of the single RCWALS structure in same structural parameters.

5. Conclusion

In this work, a simple-structure refractive index sensor that comprises a MIM waveguide and a rectangle cavity without a long side (RCWALS) is theoretically proposed. The propagation characteristics were investigated by the FEM. The results reveal that, compared with the contrastive structure, the designed single RCWALS structure has better transmission spectrum, stronger resonance, occurrence of Fano resonance at mode 1 and mode 2, which make detection easier. And it is found that the sensitivity of mode 1 is much higher than that of mode 2. Additionally, the geometric parameters were investigated. As the long side of RCWALS became larger, the dip position exhibited an apparent redshift, the shape of transmission spectra kept unaltered, the transmittance of dip got slightly higher, the sensitivity of sensing system became more excellent, and the FWHM of mode 1 varied slightly. As the short side of RCWALS got longer, the dip position almost remained unchanged, the shape changed from asymmetric narrow shape to almost symmetric broad shape, the transmittance of dip reduced, the sensitivity varied slightly, and the FWHM became larger. Hence, the best performance parameter was attained, which is the sensitivity of 1840 nm/RIU with an FOM of 51.11. Furthermore, three derived structures are presented, which comprise MIM waveguide and two RCWALS in diverse positions. Fano resonance was excited at m (1,1), m (2,1), m (1,2) of derived structure 1 and derived structure 2, whose positions differ from that at mode 1 and mode 2 of single RCWALS structure. It indicates that different structure provides diverse detection points. Derived structure 1 and derived structure 2 have lower sensitivity but higher FOM comparing with single RCWALS structure. The proposed structures are quite simple, which are easy to manufacture and apply to plasmonic nanosensors.

References

[1] W. L. Barnes, A. Dereux, and T. W. Ebbesen, “Surface plasmon subwavelength optics,” *Nature*, vol. 424, no. 6950, pp. 824–830, Aug. 2003.
[2] C. Zhao and Y. Li, “Multiple Fano resonances based on different waveguide modes in a symmetry breaking plasmonic system,” *IEEE Photon. J.*, vol. 6, no. 6, Dec. 2014 Art. no. 4802208.
[3] D. K. Gramotnev and S. I. Bozhevolnyi, “Plasmonics beyond the diffraction limit,” *Nature Photon.*, vol. 4, no. 2, pp. 83–91, Feb. 2010.

[4] Y. Yin, T. Qiu, J. Li, and P. K. Chu, "Plasmonic nano-lasers," *Nano Energy*, vol. 1, no. 1, pp. 25–41, Oct. 2011.
[5] P. Chen, R. Liang, and Q. Huang, "Plasmonic filters and optical directional couplers based on wide metal-insulator-metal structure," *Opt. Express*, vol. 19, no. 8, pp. 7633–7639, Apr. 2011.
[6] F. Ma and C. Lee, "Optical nanofilters based on meta-atom side-coupled plasmonics metal-insulator-metal waveguides," *J. Lightw. Technol.*, vol. 31, no. 17, pp. 2876–2880, Sep. 2013.
[7] S. Wang, Y. Li, Q. Xu, and S. Li, "A MIM Filter Based on a side-coupled crossbeam square-ring resonator," *Plasmonics*, vol. 11, no. 5, pp. 1291–1296, Oct. 2016.
[8] M. Fang, F. Shi, and Y. Chen, "Unidirectional all-optical absorption switch based on optical Tamm state in nonlinear plasmonic waveguide," *Plasmonics*, vol. 11, no. 1, pp. 197–203, Feb. 2016.
[9] J. Tao, Q. Wang, and X. Huang, "All-optical plasmonic switches based on coupled nano-disk cavity structures containing nonlinear material," *Plasmonics*, vol. 6, no. 4, pp. 753–759, Dec. 2011.
[10] G. Veronis and S. Fan, "Bends and splitters in metal-dielectric-metal subwavelength plasmonic waveguides," *Appl. Phys. Lett.*, vol. 87, no. 13, pp. 131102, Sep. 2005.
[11] J. Tian, R. Yang, and L. Song, "Optical properties of a Y-Splitter based on hybrid multilayer plasmonic waveguide," *IEEE J. Quantum Electron.*, vol. 50, no. 11, pp. 898–903, Nov. 2014.
[12] L. Wang, Y. Zeng, and Z. Wang, "A refractive index sensor based on an analogy T shaped metal–insulator–metal waveguide," *Optik*, vol. 172, pp. 1199–1204, Jul. 2018.
[13] L. Xu, S. Wang, and L. Wu, "Refractive index sensing based on plasmonic waveguide side coupled with bilaterally located double cavities," *IEEE Trans. Nanotechnol.*, vol. 13, no. 5, pp. 875–880, Sep. 2014.
[14] Z. Chen, J. Qi, and J. Chen, "Fano resonance based on multimode interference in symmetric plasmonic structures and its applications in plasmonic nanosensors," *Chin. Phys. Lett.*, vol. 30, no. 5, p. 057301, May 2013.
[15] X. Ren, K. Ren, and Y. Cai, "Tunable compact nanosensor based on Fano resonance in a plasmonic waveguide system," *Appl. Opt.*, vol. 56, no. 31, pp. H1–H9, Jul. 2017.
[16] I. Zand, M. S. Abrishamian, and T. Pakizeh, "Nanoplasmonic loaded slot cavities for wavelength filtering and demultiplexing," *IEEE J. Sel. Topics Quantum Electron.*, vol. 19, no. 3, pp. 4600505–4600505, Jun. 2013.
[17] T. Wu, Y. Liu, Z. Yu, Y. Peng, C. Shu, and H. Ye, "The sensing characteristics of plasmonic waveguide with a ring resonator," *Opt. Express*, vol. 22, no. 7, pp. 7669–7677, Mar. 2014.
[18] B. Yun and G. Hu, "Plasmon induced transparency in metal–insulator–metal waveguide by a stub coupled with FP resonator," *Materials Res. Express*, vol. 1, no. 3, p. 036201, Sep. 2014.
[19] J. Zhou and Z. Zhang, "Transmission and refractive index sensing based on Fano resonance in MIM waveguide-coupled trapezoid cavity," *AIP Adv.*, vol. 7, no. 1, pp. 015020, Jan. 2017.
[20] B. Zhang, L. Wang, and H. Li, "Two kinds of double Fano resonances induced by an asymmetric MIM waveguide structure," *J. Opt.*, vol. 18, no. 6, p. 065001, Jun. 2016.
[21] X. Yi, J. Tian, and R. Yang, "Tunable Fano resonance in MDM stub waveguide coupled with a U-shaped cavity," *Eur. Phys. J.*, vol. 72, no. 4, p. 60, Apr. 2018.
[22] Z. Chen, L. Yu, L. Wang, G. Duan, and J. Xiao, "Sharp asymmetric line shapes in a plasmonic waveguide system and its application in nanosensor," *J. Lightw. Technol.*, vol. 33, no. 15, pp. 1, Aug. 2015.
[23] R. Zia, J. A. Schuller, A. Chandran, and M. L. Brongersma, "Plasmonics: The next chip-scale technology," *Materials Today*, vol. 9, no. 7-8, pp. 20–27, Aug. 2006.
[24] B. Lee, H. Na and I. M. Lee, "Trapping light in plasmonic waveguides," *Opt. Express*, vol. 18, no. 2, pp. 598–623, Jan. 2010.
[25] S. Yan, M. Zhang, and X. Zhao, "Refractive index sensor based on a metal–insulator–metal waveguide coupled with a symmetric structure," *Sensors*, vol. 17, no. 12, pp. 2879, Dec. 2017.
[26] B. Yun, G. Hu, and R. Zhang, "Fano resonances in a plasmonic waveguide system composed of stub coupled with a square cavity resonator," *J. Opt.*, vol. 18, no. 5, p. 055002, May 2016.
[27] Z. Zhang, L. Luo, and C. Xue, "Fano resonance based on metal-insulator-metal waveguide-coupled double rectangular cavities for plasmonic nanosensors," *Sensors*, vol. 16, no. 5, p. 642, May 2016.
[28] R. D. Kekatpure, A. C. Hryciw, E. S. Barnard, and M. L. Brongersma, "Solving dielectric and plasmonic waveguide dispersion relations on a pocket calculator," *Opt. Express*, vol. 17, no. 26, pp. 24112–24129, Dec. 2009.
[29] H. Gai, J. Wang, and Q. Tian, "Modified Debye model parameters of metals applicable for broadband calculations," *Appl. Opt.*, vol. 46, no. 12, pp. 2229–2233, Apr. 2007.
[30] L. Chen, *et al.*, "Numerical analysis of a near infrared plasmonic refractive index sensor with high figure of merit based on fillet cavity," *Opt. Express*, vol. 24, no. 9, pp. 9975–9983, Apr. 2016.
[31] H. Wei, X. Tian, D. Pan, L. Chen, Z. Jia, and H. Xu, "Directionally-controlled periodic collimated beams of surface plasmon polaritons on metal film in Ag nanowire/Al2O3/Ag film composite structure," *Nano Lett.*, vol. 15, no. 1, pp. 560–564, Dec. 2015.
[32] F. Hu, H. Yi, and Z. Zhou, "Wavelength demultiplexing structure based on arrayed plasmonic slot cavities," *Opt. Lett.*, vol. 36, no. 8, pp. 1500–1502, Apr. 2011.
[33] K. M. Mayer and J. H. Hafner, "Localized surface plasmon resonance sensors," *Chem. Rev.*, vol. 111, no. 6, pp. 3828–3857, Jun. 2011.